Revision 1

Incorporation of chlorine in nuclear waste glasses using high-pressure vitrification: Solubility, speciation and local environment of chlorine

Valentin JOLIVET[1,2,3], Yann MORIZET*[1], Nicolas TRCERA[4], Vincent FERNANDEZ[2], Tomo SUZUKI-MURESAN[3]

[1]Nantes Université, Univ. Angers, Le Mans Université, CNRS, UMR 6112, Laboratoire de Planétologie et Géosciences, F-44000 Nantes, France

[2]Nantes Université, CNRS, Institut des Matériaux de Nantes Jean Rouxel, IMN, F-44000 Nantes, France

[3]Nantes Université, IMT Atlantique, CNRS, SUBATECH, F-44000 Nantes, France

[4]Synchrotron SOLEIL, L'Orme des Merisiers, Saint Aubin, BP 48, F-91192 Gif-sur-Yvette Cedex, France

*Corresponding author: Yann Morizet

Postal address:

Laboratoire de Planétologie et Géosciences de Nantes (LPG Nantes), UMR-CNRS 6112, Université de Nantes.

2 rue de la Houssinière, 44322 Nantes Cedex (FRANCE)

phone: +33 (0) 2 5112 5491

24 fax: +33 (0) 2 5112 5268

25 *E-mail: yann.morizet@univ-nantes.fr

ABSTRACT

The solubility, speciation and local atomic environment of chlorine have been determined for aluminoborosilicate glasses quenched from high-pressure (0.5-1.5 GPa) and high-temperature (1350-1400°C) equilibrated with various sources of chlorine (NaCl and $PdCl_2$). The Cl solubility reaches up to 11 mol.% in borosilicate glass and appears to be strongly influenced by the concentration of network modifying cations (Ca and Na) and increases with increasing $CaO + Na_2O$ content. The Cl solubility is enhanced in Ca-bearing rather than Na-bearing borosilicate glass, suggesting a higher affinity of chlorine for alkaline-earth cations. Cl K-edge XANES and Cl 2p XPS spectra reveal that chlorine dissolves in glasses only as chloride species (Cl^-) and no evidence of oxidized species is observed. Using $PdCl_2$ as a chlorine starting source leads to pre-edge signal for $PdCl_2$ in the XANES spectra. The EXAFS simulations show that Cl^- local environment is charge compensated by Na^+ or Ca^{2+} at a distance to first neighbor on the order of 2.7 Å that is comparable to the observed distances in chlorine crystalline compounds. The coordination to charge compensating cation is lower in the case of Ca^{2+} (~1.1) than Na^+ (~4.3).

Keyword

High-pressure, Chlorine, Nuclear Waste Glasses, spectroscopy.

INTRODUCTION

^{36}Cl is a long-lived and radiotoxic radioisotope (301 ky, Endt and Van der Leun 1973, Audi et al. 2017) arising from irradiated graphite in nuclear reactors (Wickham et al. 2017). ^{36}Cl is found to be a major pollutant of ground water after the Chernobyl nuclear plant accident (Chant et al. 1996, Roux et al. 2014). ^{36}Cl is mixed with stable Cl during the pyrochemical

reprocessing of spent fuel (Metcalfe and Donald 2004, Tomilin et al. 2007, Vance et al. 2012, Gin et al. 2017). The volatility of this element prevents its incorporation in common nuclear waste glass formulations with usual vitrification process in melters at ambient pressure (see Hrma 2010, Ilyukhina et al. 2010, Ojovan and Lee 2011, Gin et al. 2017, Goel et al. 2019). This behavior at high-temperature is an important obstacle owing to the ^{36}Cl high mobility in the environment, radiotoxicity and long half-life. Consequently, alternative processing should be proposed for immobilizing in a safe and permanent manner the ^{36}Cl-bearing nuclear wastes. Besides, it should be emphasized that ^{36}Cl is thought to be one of the main contributors of the dose released from geological repositories such as the CIGEO project (Meplan and Nuttin 2015). Therefore, the immobilization of chlorine is mostly dependent on the conditioning matrix durability.

A great deal of effort has been spent these last decades to develop specific glass formulations to increase chlorine retention in glasses, especially in the alkaline-earth silicate glass systems (Siwadamrongpong et al. 2004, Schofield et al. 2009, Tan 2015, Chen et al. 2017, Tan and Hand 2018, Zhao et al. 2019). Paradoxically, chlorine behavior in glasses is better known than other halogen behavior such as iodine, even though ^{129}I is of more concern than ^{36}Cl for geological disposal of nuclear wastes (Meplan and Nuttin 2015, Riley et al. 2016, Jolivet et al. 2020, 2021, Morizet et al. 2021a,b). It is due to the interest from the geological community for chlorine, as it is an important volatile species involved in the degassing of the planetary interior through magmatic processes (Johnston 1980, Symonds et al. 1988, Carroll 2005). Indeed, chlorine has a great influence on magmatic processes such as diffusion, density and viscosity; which are important to constrain for eruptive processes (Métrich and Rutherford 1992, Carroll and Webster 1994, Dingwell and Hess 1998, Aiuppa et al. 2004, Zimova and Webb 2007, Evans et al. 2008, Aiuppa et al. 2009, Filiberto and Treiman 2009, Baasner et al.

74 2013, Dalou et al. 2015, Webster et al. 2015, 2018). These works use high-pressure and high-
75 temperature conditions to increase the solubility of chlorine in melts to prevent evaporation,
76 and to allow the understanding of the dependence of chlorine solubility as a function of
77 chemical and physical parameters. For instance, it has been demonstrated that Cl solubility is
78 strongly dependent on CaO content (Carrol and Webster 1994, Signorelli and Carroll 2002,
79 Evans et al. 2008) and that Cl has strong structural affinities with Ca in glasses (McKeown et
80 al. 2011). Cl solubility is negatively affected by the Al content (Dalou et al. 2015), which may
81 be ascribed to a rivalry for the use of charge balancing cations, as observed for iodine (Jolivet
82 et al. 2020, Morizet et al. 2021b).
83 Cl solubility in borosilicate glasses is not extensively investigated, as the actual industrial
84 processes are inefficient for Cl retention in glasses at atmospheric pressure (Hrma 2010). The
85 most interesting work yet regarding chlorine behavior in borosilicate glasses is the work by
86 Tan (2015) and Tan and Hand (2018); the latter being limited to the aluminosilicate glass
87 compositions. More recently, Zhao et al. (2019) focused mostly on the role of alkaline-earth
88 cations for chlorine incorporation in glasses and concluded that i) Cl solubility in borosilicate
89 glasses increased with the size of the alkaline-earth element, the highest Cl content (2.54
90 at.%) reached for a Ba-bearing borosilicate glass, ii) the same applied to aluminosilicate
91 glasses, iii) glass composition seemed more important than melting temperature to incorporate
92 Cl in glasses, iv) Cl decreased glass transition temperature in a comparable way to other
93 halogens such as iodine (Jolivet et al. 2021) or fluorine (Zimova and Webb 2007), v) Cl
94 affected the polymerization of the glass network, as for iodine (Jolivet et al. 2020), and vi)
95 above chlorine saturation, phase separation occurred, but Cl was not necessarily present in the
96 newly formed phase, neither was it retained in the glass. Although, the aforementioned studies
97 constitute landmarked works in the race for the understanding of chlorine behavior and its

immobilization in specific glass matrices, the Cl contents reached in these nuclear waste glass could be drastically improved using pressurization vitrification. Vitrification at ambient pressure cannot prevent chlorine from escaping by evaporation, despite all the effort made to improve the process (Tan 2015, Tan and Hand 2018). Furthermore, high-pressure conditions may help to prevent phase separation, which seems to be a common issue when dealing with chlorine (see Tan 2015, Gin et al. 2017).

In the present work, we investigate the chlorine incorporation into glasses synthesized under high-pressure and high-temperature conditions. We explore borosilicate glasses with varied compositions to investigate the role of boron, the role of alkali and alkaline-earth contents in the Cl incorporation. The local atomic environment of Cl is also investigated using X-ray Photoelectron Spectroscopy (XPS) and X-ray Absorption Spectroscopy (XAS), in order to determine the impact of high-pressure conditions on the Cl environment in glasses. We also attempt to discuss the systematics of Cl solubility in glasses using a field strength formalism.

EXPERIMENTAL METHODS

Starting Material

We investigated chlorine solubility in various glass compositions in the system SiO_2-Al_2O_3-B_2O_3-CaO-Na_2O (-ZrO_2). Most of the compositions were synthesized in Jolivet et al. (2019, 2020, 2021) and Morizet et al. (2021a,b) to study the incorporation of iodine in glasses. The preparation of volatile-free glasses is described elsewhere (Jolivet et al. 2019). Glass batches were prepared from a mixture of oxides (SiO_2, Al_2O_3, CaO) and carbonates (Na_2CO_3). Prior to the high-pressure syntheses, these glasses were melted in a box furnace at 1200°C for 1 to 2 hours. Experiments on the ISG (International Simple Glass) composition were conducted from a provided ISG ingot that was also used as a standardized glass for nuclear waste glass

studies (see Gin et al. 2013). This glass has been intensively studied by the community (Inagaki et al. 2013, 2014, Elia et al. 2017, Abdelouas et al. 2013, Charpentier et al. 2016, Mendoza et al. 2012, Mohd et al. 2015, Guerette and Huang 2015, Collin et al. 2018, Jolivet et al. 2019) including for investigations on iodine incorporation in glasses using extreme conditions (Jolivet et al. 2020, 2021, Morizet et al. 2021b). All the studied glass compositions and experimental conditions are provided in the Table 1.

The ISG, LJ8 and BASN3 compositions are polymerized glasses, with a high concentration of network forming oxides (SiO_2, Al_2O_3, B_2O_3). The main difference between these glasses is mostly represented by the change in the K* parameter defined as ($[SiO_2]+[Al_2O_3]$)/$[B_2O_3]$ and modified after the K parameter from Dell et al. (1983). The ISG composition is an high silica glass (60.2 mol.% SiO_2), with 16 mol.% B_2O_3 to ease the melting and optimize the physical properties, and a small amount of Al_2O_3 and ZrO_2 stabilizing the network. The Na_2O and CaO content are optimized to balance the charges of the AlO_4^- and ZrO_6^- units, and to have a relatively high N_4 (~0.5, Charpentier et al. 2016, $N_4 = [BO_4] / [BO_4] + [BO_3]$, see Dell et al. 1983). The LJ8 composition is similar to the ISG composition, but with a lower B_2O_3 content (6.4 mol.%, Jolivet et al. 2019), and slightly more Al_2O_3, CaO, and Na_2O. Consequently, the K* of this glass, is higher than the K* of the ISG (10.8 vs 4, see Table 1). The BASN3 composition is even lower in B_2O_3 content (4.8 mol.%), and higher in SiO_2 and Al_2O_3 (64.6 and 9.8 mol.%, respectively). This glass has a higher K* than ISG and LJ8 (15.5), and the N_4 is 0.52 (see Jolivet et al. 2019). In BASN3, the Na_2O is the only non-network former (21.1 mol.% Na_2O, Table 1).

The other glasses of this study, NH, LJ4b, BFS3 and 4, C35, and the pCABS1 and 2, are depolymerized glasses, featuring low network former oxide content and relatively high non-network former content. The NH composition has been extensively used in Jolivet et al.

(2020, 2021) to investigate the effect of the incorporation of iodine in glasses. It is a simplified simulant of LAW glasses (Low Activity Waste, see Ojovan and Lee 2011), with a high Na_2O content (24.2 mol.%). It has a relatively low SiO_2 content (43.1 mol.%) and almost the same B_2O_3 content as ISG (15.1 mol.%, Table 1) but with a higher Al_2O_3 content, so the K* of NH is nearly identical to ISG (3.5 and 4, respectively). BFS3 and 4 are similar to NH, but a part of the Na_2O content is substituted with CaO (see Table 1). The pCABS1 and 2 glasses are similar to NH, but do not contain Na_2O that is replaced by CaO. The pCABS1 has a slightly different K* from pCABS2 (2.6 and 3.9, respectively) due to different B_2O_3 content (substitution with CaO content, see Table 1). The C35 is a B_2O_3 rich glass (29.1 mol.%), that does not contain Na_2O (33.6 mol.% CaO) and has been studied in Morizet et al. (2021a). It has one of the lowest K* with LJ4b (1.3 and 1.5, respectively). LJ4b has an intermediate SiO_2 content (49.8 mol.%), an high B_2O_3 content (33.8 mol.%), and a high Na_2O content (16.4 mol.%, Table 1). The N_4 of this glass is 0.42 (in Jolivet et al. 2019). Overall, the investigated glass compositions probe a large range of B_2O_3 (5-35 mol.%), large range of SiO_2 (30-65 mol.%) and a large range of network modifying cations (9-33 mol.%) with either CaO or Na_2O or both as the nature of network modifying cation.

High-pressure syntheses

The experimental charge consists of a mix of glass powder (~300 mg) and a Cl-bearing compound (~30 mg), such as NaCl or $PdCl_2$. The NaCl is dried at 500°C for 24 h in a box furnace prior to loading. We also use $PdCl_2$ as Pd and Cl_2 dissociates at high-temperature, and Pd is poorly soluble in glasses, as described in Dalou et al. (2015). In all cases, chlorine is loaded above supposed saturation and Cl input can be as high as 29.1 mol.% (Table 1). The mixed powder is loaded into platinum capsules (13 mm in length and 5.4 mm in diameter) welded shut at both ends. The capsule is isolated from the graphite furnace with a MgO

ceramic sleeve. The intrinsic oxygen fugacities (fO_2) are supposed to be constrained by the used ¾ inch talc-Pyrex assemblies at relatively oxidizing conditions (Morizet et al. 2017) at 1.5 log unit above the Quartz-Fayalite-Magnetite (QFM) buffer.

High-pressure experiments are achieved using an end-load piston-cylinder apparatus, following the same protocol as described in Jolivet et al. (2020). Sample pressure is first increased to 0.5 GPa, then temperature is increased to ~500°C and held for 5 min for NaCl loaded syntheses, to an hour for $PdCl_2$ loaded syntheses to allow the dissociation of NaCl and $PdCl_2$, into Cl, Na and Pd, respectively. Then, pressure and temperature are increased to the final conditions. Experimental conditions for each synthesis are presented in the Table 1. We investigated a pressure range from 0.5 to 1.5 GPa, and a temperature range from 1300 to 1500°C. The temperature was monitored with a B-type thermocouple measuring at the top of the capsule. The measured temperature has a precision of ±5°C. Most of the experiment were melted for 5h. We performed an isobaric quench, using a piloted pumping system. The quench rate is at least ~100°C/s in the first 500°C.

Scanning Electron Microscopy – Energy Dispersive Spectroscopy (SEM-EDS) for major element concentrations in glasses

The chemical characterization of the recovered glasses was performed with a JEOL 5800LV SEM, equipped with a SDD SAMx EDS. The glass chips were mounted in an epoxy plug, with an ISG reference chip on each plug. We used ISG (Gin et al. 2013, Table 1), as a standard composition to ensure the correctness and robustness of the analytical measurements. The electron beam voltage was set at 15 kV and the current at 0.5 nA. The current was regularly controlled to ensure a reproducible electron flow during all the analytical campaigns. The acquisitions were conducted on a spot larger than 20 µm to avoid Na loss under the electron beam. We followed the recommendations of Newbury and Ritchie (2013)

to improve the quality of our results. Each sample was scanned at least 10 times with a scan duration of 1 min to reduce the minimum concentration for identification (peak threshold criterion, see Newburry and Ritchie 2013). We used the minor X-ray family members to avoid misinterpretation near noise level and improve the quantification. We started and finished all analytical measurements with 15 scans of an ISG sample to ensure there was no instrumental drift. All the measurements were obtained using internal standards for the different elements: LaB_6 for B_2O_3, wollastonite for SiO_2 and CaO, NaCl for Na and Cl, Corundum for Al_2O_3. The EDS results were slightly corrected in accordance with the ISG standard composition given by Gin et al. (2013). Based on the replicated measurements, the uncertainty of the major oxide and chlorine quantification was typically ± 0.2 mol.%. All chemical characterization results are shown in the Table 1.

X-ray Photoelectron Spectroscopy (XPS) for chlorine speciation in glasses

Several glass samples were investigated using XPS to determine the chlorine speciation. Spectrum acquisition was carried out on a Kratos Nova spectrometer equipped with a monochromatic Al Kα radiation operating at 1486.6 eV and 300 W. The characterization (beam size 300x700 μm^2) was done on glass chips collected from the bulk of the experimental charge (3x3 mm^2). We acquired the spectra with different pass energy: at 160 eV for the wide spectrum with a step of 0.5 eV and at 20 eV for high-resolution XPS spectra on elements with a step of 0.1 eV. The all over XPS instrument energy resolution with the pass energy 160 and 20 eV was on the Fermi edge 1.9 and 0.4 eV, respectively. All measurements were conducted with charge neutralization owing to the insulating nature of the glass samples. The spectra were referenced against the adventitious C 1s transition at 284.8 eV. For Cl species, the high-resolution XPS spectra were acquired at the Cl 2p ~200 eV binding energy core level and with a spectral window between 190 and 215 eV to be sufficiently large for background

subtraction and to cover the region for chloride (~199 eV) and chlorate (~208 eV) species (Moulder et al. 1992). We used the CasaXPS© software to treat the XPS spectra (Fairley et al. 2021). We used a Tougaard function for background subtraction (Tougaard 1997). For each local Cl environment, the Cl 2p peaks were fitted with two asymmetric Gaussian-Lorentzian lines linked to keep the area ratio of 1/2 between the $2p_{3/2}$ and $2p_{1/2}$ lines and a spacing of 1.6 eV in agreement with spin-orbit splitting ratio.

X-ray Absorption Spectroscopy (XAS)

For several glass samples, we acquired the Cl K-edge X-ray Absorption Spectroscopy. The acquisitions were conducted on the LUCIA beamline at SOLEIL synchrotron operating at a current of 450 mA and an energy of 2.75 GeV (Vantelon et al. 2016). Both the X-ray Absorption Near-Edge Spectroscopy (XANES) and Extended X-ray Absorption Fine Structure (EXAFS) regions were acquired. The energy of the incoming photons was selected by using double crystal monochromator Si(111). The energy calibration of the incoming photons was achieved on NaCl powder by selecting the first inflexion point of the spectrum at 2824.5 eV. The XAS spectra on the glass were collected in fluorescence mode with a silicon drift diode detector. To avoid the self-absorption effect, the geometry of the beamline was set to a low angle between the sample surface and the detector (2°).

During the experiment, the spectra were acquired with an unfocused beam having a size of 4x2 mm^2 in order to maximize the count rate. The glass powder was placed on a copper plate using carbon tape and placed inside a vacuum chamber at $5x10^{-2}$ mbar. The XAS spectra were collected at the Cl K-edge in the range 2780-3800 eV. For each point, the counting time could go up to 10 s depending on the region of interest. We collected at least five spectra on each glass sample in order to obtain an average spectrum with a good signal to noise ratio. The

241 presented spectra correspond to an average of the different scans for a given sample. We also
242 conducted acquisition on several crystalline standards for comparison and fingerprinting of
243 the XAS glass spectra: NaCl, $CaCl_2$, $PdCl_2$, $NaClO_4$. In these crystalline compounds, the Cl
244 oxidation state varies from -1 in chlorides to +7 in perchlorates, and the local environment of
245 Cl is changing with respect to the first coordination shell (i.e. distance and coordination
246 number to the first neighbor).

247 The XAS spectra were reduced using the Demeter package; the normalization and the merge
248 of the XAS spectra as well as the background removal were carried out with the Athena
249 software (Newville et al. 1995; Ravel and Newville 2005) or Fastosh (Landrot 2018). In
250 addition, the self-absorption effect was checked using the Fluo algorithm implemented in
251 Athena. For several samples (i.e. the ones synthesized with $PdCl_2$ as the source of Cl), we had
252 to correct the XANES spectra with the Athena deglitching package, due to the presence of
253 several absorption peaks related to the presence of Pd and located at 3173 eV (L_3-edge) and
254 3330 eV (L_2-edge). The description of the spectrum treatment is provided in Suppl. Mat. 2.

255 The first coordination sphere to Cl atoms was obtained from the simulation of the EXAFS
256 signal by using the single scattering signals determined by known crystalline structure: NaCl,
257 $CaCl_2$ and $PdCl_2$, and obtained from the Crystallographic Open Database (Vaitkus et al.
258 2021). We used k^2-weighted signal function in the k-space between 2.85 and 8.5 $Å^{-1}$ for all
259 spectra. The simulation of the Radial Distribution Function (RDF) using the scattering paths
260 was done using the Artemis software. We used the spectrum from $NaClO_4$ to determine the
261 delta E_0 (ΔE_0 = -3.8 eV) and the scattering amplitude (S_0^2 = 0.888). We used different RDF
262 interval (1.1-3.0 Å) depending on the sample (see Table 2).
263

RESULTS

Cl solubility in borosilicate glasses

The recovered high-pressure glasses were examined for crystals or bubbles. Samples with strong heterogeneities were discarded from the study (i.e. samples showing phase separation). Samples with bubbles are common and kept, as the presence of bubbles assesses the saturation of chlorine in the glass. If most of the samples are transparent, several samples also exhibit a tainted brown color. For instance, the brownish color observed for C35-Cl is ascribed to the presence of tiny bubbles. We did not find Pd micro-sphere as observed in Dalou et al. (2015). We assume that most of the Pd stayed at the bottom of the capsules during the experiment, due to the way it was loaded (at the bottom instead of mixed), the high density of Pd and because of the low viscosity of borosilicate melts at >1000°C. However, as mentioned above the XAS spectra show evidence of Pd absorption peaks, which implies that some Pd is still present in the bulk glass. The content of the bubbles could not be analyzed but is assumed to be Cl_2 gas. The chlorine content in the glasses is presented in the Table 1.

We performed experiments mostly at 1 GPa and at 1400°C to focus this study on glass compositional parameters. The Cl content as a function of non-network cation concentration, expressed as the [CaO + Na_2O] is shown in Figure 1 and is obtained from the data point in Table 1. The change in Cl solubility as a function of K* as described earlier is provided in the Suppl. Mat. 2 as it turns out to be less informative than anticipated. The distinction has been made for the samples obtained with NaCl and $PdCl_2$ as the source of chlorine and as a function of pressure (0.5 to 1.5 GPa). In Figure 1, within the error in the chlorine content (±0.2 mol.%) we do not identify any effect of the initial source of chlorine. The Cl content in glasses appears strongly dependent on the non-network cation content. For instance, the lowest Cl content reached (~2 to 4 mol.%) are for the ISG composition having a low [CaO +

288 Na_2O] content; whereas the highest Cl content is observed for C35-Cl (11.1 mol.% Cl) and
289 pCABS2-Cl (~10 mol.% Cl) having high CaO content (~30 mol.%). The observed trend is not
290 surprising as Cl is thought to be incorporated in the vicinity of these cations, especially
291 alkaline-earth cations (McKeown et al. 2011, Tan 2015, Tan and Hand 2018, Zhao et al.
292 2019). The nature of the non-network forming cation should play a role as well. For instance,
293 Cl content in NH, BFS4 and BFS3 samples is increasing along with the substitution of Na for
294 Ca (see Table 1) for experiments loaded with NaCl and conducted at 1.0 GPa. The same is
295 observed for polymerized glasses such as LJ8 and BASN3: BASN3 contains only Na_2O (21.1
296 mol.%), whereas LJ8 also contains CaO (9 mol.%, plus 15.3 mol.% Na_2O), the latter is richer
297 in Cl than BASN3 of 1 to 2 mol.% (Table 1).

298 The Figure 2 presents the Cl content as a function of the XCaO defined as [CaO] / [CaO +
299 Na_2O]. The results shows that Cl content is positively correlated with the XCaO. The highest
300 Cl content is reached for the highest XCaO compositions, such as C35-Cl at 11.1 mol.% Cl
301 (XCaO = 1, see Table 1). Conversely, the lowest Cl content is observed in the Ca-free
302 compositions, such as BASN3 (from 1.1 to 3.4 mol.% Cl) and LJ4b (4 mol.% Cl, Table 1,
303 Figure 2). Compositions with similar XCaO (ISG and NH, Table 1) exhibit higher Cl content
304 when depolymerized (CaO + Na_2O content is higher). Compositions with similar K*
305 parameters, such as the NH, BFS4 and BFS3 series, solubilize more Cl with increasing
306 XCaO: 3.5 to 6.4 for NH (XCaO ~ 0.24), 6.5 for BFS4 (XCaO ~ 0.64), to 10.2 for BFS3
307 (XCaO ~ 0.83, see Table 1 and Figure 2). In lime glasses (pCABSx and C35), the Cl content
308 increases with both B_2O_3 content and CaO content, from 21.8 mol.% B_2O_3 and 16.1 mol.%
309 CaO for pCABS1-Cl, to 29.7 mol.% B_2O_3 and 26.2 mol.% CaO for C35-Cl. This is consistent
310 with the conclusion of Evans et al. (2008) and McKeown et al. (2011), which mention that Cl
311 has more affinities with Ca^{2+} in glasses than with Na^{+} cations. At first sight (from Figure 1

and 2), we do not observe a clear impact of the initial source of chlorine (NaCl or $PdCl_2$) on the chlorine solubility, however, this aspect requires more experimental investigations to be clarified.

Chlorine speciation in borosilicate glasses from XPS and XANES

Several glasses were characterized using Cl K-edge XAS. The Cl XANES for the studied glasses and crystalline chlorine compounds are shown in Figure 3A and B, respectively. The spectra for glasses have been categorized as a function of loaded chlorine source: NaCl or $PdCl_2$. There is a striking feature observed in Figure 3A that is the presence of a pre-peak located at ~2821 eV for the samples synthesized with $PdCl_2$ source. This peak is absent in the spectra for samples synthesized with NaCl. The same pre-peak is observed in the spectrum obtained for $PdCl_2$ in Figure 3B, which suggests that a non-negligible quantity of $PdCl_2$ is present in the glass. Whether it corresponds to dissolved or disseminated $PdCl_2$ particles is not clear and would require advanced characterization using Transmitted Electron Microscopy to investigate at the nanoscale the glasses.

As shown in Figure 3B, there is a clear distinction between chlorine species depending on the Cl oxidation state. For instance, the main line for reduced Cl in crystalline compounds (-1 in NaCl, $CaCl_2$ and $PdCl_2$) is located at ~2828 eV whereas the main line for oxidized Cl in crystalline compounds (+7 in $NaClO_4$) is located at ~2834 eV. The shift to higher energy in the edge position is a common feature that has been documented in previous work for other elements such as Fe (e.g. Wilke et al. 2011). For crystalline compounds, the main line is broad in the case of NaCl and $CaCl_2$ and narrower for $NaClO_4$. The latter spectrum exhibits a broad signal between 2840 and 2860 eV that is not visible in the spectra for NaCl and $CaCl_2$ or $PdCl_2$. Without exception, the spectra obtained for glasses in Figure 3A show a main line

335 relatively broad and asymmetric with a peak maximum at 2828 eV, regardless of the initial
336 source of chlorine and the existence of the pre-peak due to the presence of $PdCl_2$. This
337 observation clearly indicates that chlorine is dissolved under its reduced form, Cl^-, within the
338 glass structure and surrounded by either Na^+ or Ca^{2+} as charge balancing cation, or even Pd^{2+}
339 in the case of samples synthesized with $PdCl_2$ as the initial source of chlorine. This result is in
340 total agreement with the previous work using XANES from Evans et al. (2008) on
341 aluminosilicate glasses synthesized at high pressure (0.5 GPa). McKeown et al. (2011) also
342 pointed out that chlorine was dissolved as Cl^- with Ca^{2+} as the main balancing cation based on
343 EXAFS simulation of the first coordination sphere for chlorine in borosilicate glasses
344 synthesized at ambient pressure.

345 The suggested results from XANES analyses are confirmed by the XPS analyses that are
346 shown in Figure 4 for several samples. The entire set of spectra is provided in the Suppl. Mat.
347 1. We show in Figure 4 the XPS spectra obtained in the Cl 2p energy region along with the
348 modeling of the $2p_{3/2}$ and $2p_{1/2}$ peaks and the derived peak parameters. The nature of the
349 chlorine source and the measured Cl content is reported on each plot. First, the nature of
350 initial chlorine does not seem to influence the measured Cl speciation. Second, for all the
351 characterized samples there is only one peak doublet that is ascribed to the Cl $2p_{1/2}$ and $2p_{3/2}$
352 located at 201 and 198 eV, respectively. The derived peak width at half maximum is on the
353 order of 1.5 eV and the peak position are 198.7 and 200.3 eV for the Cl $2p_{3/2}$ and $2p_{1/2}$,
354 respectively. The chlorine signal located at this binding energy corresponds to chlorine
355 dissolved as chloride species: NaCl, $CaCl_2$ and $PdCl_2$ in our case and as reported in Moulder
356 et al. (1992). Distinction between the chloride species is currently not possible from the
357 spectra in Figure 4. The chloride is the only species and there is no evidence for chlorate
358 species that would give a peak doublet between 205 and 210 eV (Moulder et al., 1992);

359 therefore, confirming the XANES results and in agreement with previous works on the
360 chlorine dissolution in glasses (Evans et al. 2008, McKeown et al. 2011). Both XANES and
361 XPS results are essential and complementary as they provide constraints on the employed
362 model that will be used for determining the geometry of the local Cl environment in glasses
363 using EXAFS simulation.

364 **Chlorine local environment in borosilicate glasses from Cl K-edge EXAFS simulations**

365 The results of the EXAFS simulations for several samples are reported in Figure 5 showing
366 the total amplitude of the EXAFS signal ($|\chi(R)|$ in $Å^{-3}$) as a function of the RDF ($R+\Delta R$ in Å).
367 The fitted curve to the data is shown as well as the RDF region that is of concern for the fit
368 (see Table 2). An insert of the imaginary part ($|\chi(R)$ Img| in $Å^{-3}$) of the amplitude is also
369 shown (the entire set of spectra is provided in Suppl. Mat. 1). It should be pointed out that the
370 shown EXAFS spectra is corrected to remove a low RDF signal ($R+\Delta R < 1.6$ Å) that does not
371 correspond to a chlorine signal. Details on the correction procedure is provided in Suppl. Mat.
372 2. Currently, we do not have any explanation for the presence of this low RDF signal. The
373 XANES and XPS results show that chlorine dissolves as chloride species (NaCl, $CaCl_2$ and
374 $PdCl_2$). For chlorides, the typical next nearest neighbor distance is the lowest at 2.31 Å for
375 $PdCl_2$ (Wells et al. 1938) and is on the order of ~2.70 Å for NaCl and $CaCl_2$ (van Bever and
376 Nieuwenkamp 1935, Finger et al. 1978). Owing to the mathematical form of the EXAFS
377 function, such distances correspond to peak position at ~1.8 and 2.2 Å for $PdCl_2$ and NaCl or
378 $CaCl_2$, respectively. Therefore, signals below this region do not actually correspond to a
379 possible chlorine local environment present in the investigated borosilicate glasses. The
380 $R+\Delta R$ signal obtained for C35-Cl is a particular case (see Figure 5E) as the signal at low
381 radial distribution function ($R+\Delta R < 1.5$ Å) is not averaged out by the applied correction. The

peak located at ~1.4 Å could correspond to a first nearest neighbor distance close to ~1.9 Å. That distance could match adequately to the Cl-Cl distance in Cl_2 molecules (Karan and Arunan 2004). One can argue that the EXAFS signal at lower R+ΔR could also correspond to next nearest neighbor in chlorate (or perchlorate) cluster, in which a Cl^{5+} is surrounded by three oxygen atoms for charge compensation at typical distance of ~1.4 Å (Zachariasen 1929); however, we have demonstrated that chlorate species are absent from the synthesized borosilicate glasses.

The simulation of the EXAFS signal has been performed using the following single scattering paths: Cl-Na, Cl-Ca and Cl-Pd. The Cl-Pd scattering path was not used in the case NaCl was the initial source of chlorine; the Cl-Na scattering path was not used in the case of Na-free glasses (pCABS2 and C35); the Cl-Ca scattering path was not used in the case of Ca-free glasses (BASN3-212 and LJ4b). We used $r_{Cl\text{-}Na}$, $r_{Cl\text{-}Ca}$ and $r_{Cl\text{-}Pd}$ at 2.72, 2.70 and 2.31 Å. For each scattering path, we started with a Debye-Waller factor ($\sigma_{Cl\text{-}X}$) of 0.003 and fixed the coordination numbers ($CN_{Cl\text{-}X}$) at 1. The optimization of the EXAFS spectra was done with the following steps: the $r_{X\text{-}Cl}$ was optimized then followed by the $\sigma_{Cl\text{-}X}$; this step was repeated two to three times, then the $CN_{Cl\text{-}X}$ was optimized. The entire optimization procedure was repeated several times. The optimization was stopped when parameters did not show any significant improvement in the χ^2 value (χ^2 witnessing the robustness of the fit). It should be stressed that the reported simulation represents only one possible solution and that other solutions may exist.

The simulation results are provided in Table 2. The reported error bars have been determined from the Artemis software. We did not observe any systematic change of the derived parameters ($CN_{Cl\text{-}X}$, $r_{Cl\text{-}X}$ and $\sigma_{Cl\text{-}X}$) as a function of chlorine content. The derived distances to the next nearest neighbor are on average 2.29±0.13, 2.64±0.07 and 2.75±0.04 Å for Cl-Pd, Cl-

406 Na and Cl-Ca, respectively. These distances are comparable to the observed distances in
407 crystalline structures for chlorides and in good agreement with the results of Chungong et al.
408 (2017) based on neutron diffraction data. However, the obtained r_{Cl-X} distances are
409 significantly different from the results reported in McKeown et al. (2011) that extracted r_{Cl-Na}
410 close to 4 Å. The same applies to the CN_{Cl-Na} that is on the order of 8 in McKeown et al.
411 (2011) whereas it is on average 4.3 from the results in Table 2. Although it is difficult to
412 reconcile both sets of results, we point out that the proposed results in Table 2 and Figure 5
413 are a non-unique solution. The CN_{Cl-Ca} is on average 1.08 that is ¼ of the derived CN_{Cl-Na}.
414 This difference is potentially explained by the change in the cationic charge: less Ca^{2+} than
415 Na^{+} is required to charge compensate the Cl^{-}. The CN_{Cl-Na} is surprisingly high in the case of
416 NH22-2, respectively. We currently do not have any explanation for such a high CN_{Cl-Na}. One
417 hypothesis is that regions within the NH glass are enriched with respect to Na while others are
418 depleted, and Cl^{-} aggregates several Na^{+} for charge compensation. To our knowledge, these
419 results are the first obtained on the chlorine local environment in Cl-bearing borosilicate
420 glasses synthesized under high-pressure conditions; however, more advanced experimental
421 work is required to provide a full picture of the local atomic environment for chlorine
422 dissolved in glasses under different conditions: from reduced (Cl^{-}) to fully oxidized (Cl^{7+}).

423

424 **IMPLICATIONS: RATIONALE FOR CHLORINE SOLUBILITY IN**
425 **ALUMINOBOROSILICATE GLASSES**

426 Chlorine solubility results shown in the present work suggest that high-pressure conditions are
427 beneficial for dissolving large amount of chlorine in the glass. Whereas this behavior has been
428 observed for aluminosilicate glasses previously (Alletti et al. 2009, Dalou et al. 2015, Webster

et al. 2014, 2015), we also show it for aluminoborosilicate glasses with application to the immobilization of chlorine nuclear waste. It should be mentioned that the determined Cl content is higher than the I content reached in Jolivet et al. (2020) and Morizet et al. (2021a) for identical glass compositions (i.e. ISG, NH, C35), which confirms once more that there is a solubility hierarchy between halogens related to their size (Dalou et al. 2015, Dalou and Mysen 2015). In addition, chlorine solubility appears to be affected by the nature of the charge compensating cation as observed in Figure 2 and showing a strong increase in Cl solubility with increasing XCaO. This result suggests that increasing the cation charge for the Cl^- charge compensating element induces an increase in the chlorine solubility. Zhao et al. (2019) showed that changing the alkaline-earth cation also changes the chlorine solubility. These aspects imply that chlorine solubility is to some extent controlled by the nature of the charge compensating cation and that Cl^- is better dissolved in the vicinity of alkaline-earth cations.

We have synthesized this aspect in Figure 6 compiling several experimental datasets obtained on chlorine solubility. We did not gather all the existing experimental data points, however, these represents a good picture of the Cl solubility as a function of glass composition. We compiled the data 1) from Filiberto and Treiman (2009) obtained on a basaltic composition synthesized under reducing conditions; 2) from Dalou et al. (2015) investigating the effect of Al_2O_3 content on the Cl solubility in simplified Na_2O/K_2O-Al_2O_3-SiO_2 system for pressure between 0.5 and 2.5 GPa; 3) from Webster et al. (2015) that were obtained for pressure up to 0.7 GPa under oxidizing and anhydrous conditions; and 4) from the present work acquired between 0.5 and 1.5 GPa and for aluminoborosilicate glass compositions. The change in the glass composition is expressed as the Network Modifying Field Strength that is calculated with the following equation (1):

$$Net.Mod.Field\ Str. = \frac{\sum_i \frac{z_i}{r_i} \times X_i}{\sum \frac{2}{r_{O^{2-}}} \times X_{O^{2-}}} \quad (1)$$

Where X_i corresponds to the molar fraction of network modifying cation i (i.e. Na^+, K^+, Ca^{2+} and Mg^{2+} in the present database), z_i/r_i is the cation field strength defined as the ratio between the effective cationic charge divided by the cation radius. We used the data from Shannon (1976) for r_i. The dividing term is calculated from the sum of the oxygen molar fraction on network modifying oxides.

In detail, several trends or data distributions can be observed from Figure 6. The reported data points from Filiberto and Treiman (2009) at the lower right in Figure 6 suggest that imposing reducing conditions (graphite capsules corresponding to log fO_2 at QFM -1.5, Quartz-Fayalite-Magnetite buffer, relevant to martian magmatism, e.g. Herd et al. 2002) induces an observable decrease in Cl solubility. The observed lower Cl solubility under reducing conditions is comparable to the behavior observed for CO_2 (Pawley et al. 1992, Morizet et al. 2010, Wetzel et al. 2013) or S (Jugo et al. 2010, Klimm et al. 2012). The main difference is that imposing reducing experimental conditions imposes to reduce the volatile species: CO_2 reduced to CO, CH_4; S reduced to S^{2-}. It is not the case for chlorine considering that Cl^- is the most reduced chlorine species. Applying reducing conditions involve a change in the melt structure by redistributing the network modifying cations that are possibly less available for charge compensation of the negative charges for Cl^- that cannot dissolves.

The data of Dalou et al. (2015), trends on the left with increasing Al content, shows that: 1) there is a dramatic effect of the glass Al content on chlorine solubility with a maximum Cl solubility in Al-free glasses, 2) at a given composition increasing pressure induces an increase in the Cl solubility, and 3) increasing the cation field strength induces an increase in the Cl

475 solubility. The decrease in Cl solubility with increasing Al_2O_3 content can be explained by the
476 fact that Al species (i.e. AlO_4^-) in the glass require charge compensation by network
477 modifying cation due to the excess negative charge on AlO_4^- units. A comparable behavior
478 has been observed for iodine dissolved as I^- in borosilicate glasses (Jolivet et al. 2020, Morizet
479 et al. 2021b): the charge compensating cation for AlO_4^- units is not scavenged by the
480 dissolution of I^- species therefore limiting the iodine solubility. It can also be observed that
481 the Cl solubility is affected by the nature of the alkali itself and that a distinct trend in Cl
482 solubility can be observed for K-bearing and for Na-bearing glasses. We suspect that the
483 difference in the z_i/r_i between K^+ and Na^+: 0.725 and 0.980, respectively; could explain such
484 difference in Cl solubility: Increasing the z_i/r_i value would increase the Cl solubility. Our data
485 obtained on Ca-bearing glasses (Ca^{2+} with $z_i/r_i = 2$) show the highest Cl solubility above 10
486 mol.%.

487 The data from Webster et al. (2015) shown in Figure 6 exhibit an exponential increase in the
488 Cl solubility with increasing Network Modifying Field Strength, regardless of the
489 experimental conditions. Our data on aluminoborosilicate glasses also match the trend shown
490 by Webster et al. (2015) data. The glass compositions investigated in Webster et al. (2015)
491 have ~10 mol.% Al_2O_3 at the lowermost end of the Dalou et al. (2015) trends with ~11 mol.%
492 Al_2O_3. Most of the Cl solubility points are obtained on glasses having network former cation
493 concentrations (i.e. SiO_2, Al_2O_3 and B_2O_3) on the order of ~60 to 70 mol.%. C35-Cl has less
494 than 50 mol.% for SiO_2+Al_2O_3+B_2O_3 and also has the highest Cl solubility obtained.
495 Therefore, the nature and the concentration of network modifying cation appear to be of a
496 prime importance for the dissolution of chlorine. Depolymerizing the glass structure by
497 increasing the network modifying cation concentration allows the dissolution of more chlorine
498 as Cl^-. This is consistent with the high concentration of chlorine measured in natural silica

499 undersaturated rocks (Paul et al. 1976). Large interest in chlorine behavior has been raised
500 from previous experimental studies (Webster et al. 1999, 2014, 2015, 2020); however, further
501 additional work is required to build semi empirical model for chlorine solubility that can
502 integrate a broader range of glass compositions, from aluminosilicate to aluminoborosilicate
503 glasses, held under various pressure, temperature and redox conditions.

504

505 **SUMMARY**

506 In the present work, we have investigated the solubility, the speciation, and the local atomic
507 environment of chlorine in aluminoborosilicate glasses synthesized under high-pressure
508 conditions (0.5-1.5 GPa). The XPS and XANES measurements reveal that chlorine is
509 dissolved as chloride (Cl^-) species in the glass. The EXAFS fitting of the Cl spectra show that
510 the Cl^- local atomic environment is surrounded by Na^+ or Ca^{2+} at distances on the order of
511 ~2.7 Å. Furthermore, four times as much Na^+ than Ca^{2+} is required to charge compensate the
512 chloride negative charge.

513 We also show that chlorine dissolution is strongly favored in Ca-rich glass composition over
514 Na-rich ones. Comparison with previous experimental data on Cl solubility indicates that
515 describing the Cl solubility evolution as a function of glass composition is rather complex and
516 involves several aspects: 1) the nature of the Cl^- charge compensating cation, 2) the
517 concentration of Al_2O_3 that requires charge compensation, 3) the fO_2 conditions whether it is
518 oxidizing or reducing and then 4) the degree of polymerization of the glass that allows the
519 insertion of chlorine within its structure.

520

ACKNOWLEDGEMENT

The authors are grateful to the Région Pays de la Loire, which financed the current work through the Pari Scientifque "CIPress". The authors thank the Laboratoire de Planétologie et Géosciences, the Institut des Matériaux Jean Rouxel, the Nantes Université and the CNRS for providing access to the analytical facilities. We acknowledge SOLEIL for provision of synchrotron radiation facilities and we would like to thank LUCIA staff for assistance in using the beamline. We also thank Nicolas Stéphant for support on the SEM/EDS analytical platform. We would like to thank Don Baker for handling our manuscript and the two anonymous reviewers for their fruitful comments that helped to improve the quality of the manuscript.

References

Abdelouas, A., El Mendili, Y., Aït Chaou, A., Karakurt, G., Hartnack, C., Bardeau, J.-F., Saito, T., and Matsuzaki, H. (2013) A preliminary investigation of the ISG glass vapor hydration. Journal of Applied Glass Science, 4, 307-316.

Aiuppa, A., Federico, C., Giudice, G., Guerrieri, S., Paonita, A., and Valenza, M. (2004) Plume chemistry provides insights into mechanisms of sulfur and halogen degassing in basaltic volcanoes. Earth Planetary Science Letter, 222, 469–483.

Aiuppa, A., Baker, D.R., and Webster, J.D. (2009) Halogens in volcanic systems. Chemical Geology, 263, 1-18.

Alletti, M., Baker, D.R., and Freda, C. (2009) Halogen diffusion in a basaltic melt. Geochimica and Cosmochimica Acta, 71, 3570-3580.

Audi, G., and Wang, M. (2017). The NUBASE 2016 evaluation of nuclear properties. 41, 1–138.

Baasner, A., Schmidt, B.C., and Webb, S.L. (2013) Compositional dependence of the rheology of halogen (F, Cl) bearing aluminosilicate melts. Chemical Geology, 346, 172–183.

van Bever, A.K., Nieuwenkamp, W. (1935) Die Kristallstruktur von Calciumchlorid, Ca Cl_2 Zeitschrift fuer Kristallographie, Kristallgeometrie, Kristallphysik, Kristallchemie, 90, 374-376.

Carroll, M.R., and Webster, J.D. (1994) Solubilities of sulfur, noble gases, nitrogen, chlorine and fluorine in magmas. In Volatiles in Magmas, vol. 30 (eds. M. R. Carroll and J. R. Holloway). Reviews in Mineralogy, pp. 231–279.

Carroll, M.R. (2005) Chlorine solubility in evolved alkaline magmas. Annals of Geophysics, 48, 619–631.

Cicconi, M.R., Pili, E., Grousset, L., Florian, P., Bouillard, J.C., Vantelon, D., and Neuville, D.R. (2019) Iodine solubility and speciation in glasses. Scientific Report, 9, 7758.

Chant, L.A., Andrews, H.R., Cornett, R.J., Koslowky, V., Milton, J.C.D., Van der Berg, J.G., Verburg, T.G., and Wolterbeek, H.T. (1996) ^{129}I and ^{36}Cl concentrations in lichens collected in 1990 from three regions around Chernobyl. Applied Radiation and Isotopes, 47, 933-937.

Charpentier, T., Martel, L., Mir, A.H., Somers, J., Jégou, C., and Peuget, S. (2016) Self-healing capacity of nuclear glass observed by NMR spectroscopy. Scientific Report, 6, 25499.

Chen, X., Karpukhina, N., Brauer, D.S., and Hill, R.G. (2017). High chloride content calcium silicate glasses. Physical Chemistry Chemical Physics, 19(10), 7078–7085.

Chungong, L.F., Swansbury, L.A, Mountjoy, G., Hannon, A.C., Lee, A.F., and Martin, R.A. (2017) Atomic structure of chlorine containing calcium silicate glasses by neutron diffraction and ^{29}Si solid-state NMR. International journal of Applied Glass Science, 8, 383-390.

567 Collin, M., Fournier, M., Frugier, P., Charpentier, T., Moskura, M., Deng, L., Ren, M., Du, J.,
568 and Gin, S. (2018) Structure of International Simple Glass and properties of passivating layer
569 formed in circumneutral pH conditions. Nature Material Degradation, 2, 4-16.
570 Dalou, C., and Mysen, B.O. (2015) The effect of H_2O on F and Cl solubility and solution
571 mechanisms of in aluminosilicate melts at high pressure and high temperature. American
572 Mineralogist, 100, 633–643.
573 Dalou, C., Le Losq, C., Mysen, B.O., and Cody, G.D. (2015) Solubility and solution
574 mechanisms of chlorine and fluorine in aluminosilicate melts at high pressure and high
575 temperature. American Mineralogist, 100, 2272-2283.
576 Dell, W.J., Bray, P.J., and Xiao, S.Z. (1983) ^{11}B NMR studies and structural modeling of
577 Na_2O-B_2O_3-SiO_2 glasses of high soda content. Journal of Non-Crystalline Solids, 58, 1-16.
578 Dingwell, D.B., and Hess, K.-U. (1998) Melt viscosities in the system Na-Fe-Si-O-F-Cl:
579 Contrasting effects of F and Cl in alkaline melts. American Mineralogist, 83, 1016–1021.
580 Du, L.S., and Stebbins, J.F. (2005) Network connectivity in aluminoborosilicate glasses: a
581 high-resolution ^{11}B, ^{27}Al and ^{17}O NMR study. Journal of Non-Crystalline Solids, 351, 3508–
582 3520.
583 Elia A., Ferrand K., and Lemmens K. (2017) Determination of the forward dissolution rate for
584 international simple glass in alkaline solutions. MRS Advance, 12, 661-667.
585 Endt, P.M., and Van der Leun, C. (1973) Energy levels of a ¼ 21-44 nuclei (V). Nuclear
586 Physics A, 214, 1-625.
587 Evans, K.A., Mavrogenes, J.A., O'Neill, H.St.C., Keller, N.S., and Jang, L.-Y. (2008) A
588 preliminary investigation of chlorine XANES in silicate glasses. Geochemistry, Geophysics,
589 Geosystems, 9, 15 p.

590 Fairley, N., Fernandez, V., Richard-Plouet, M., Guillot-Deudon, C., Wlaton, J., Smith, E.,
591 Flahaut, D., Greiner, M., Biesinger, M., Tougaard, S., Moorgan, D., and Baltrusaitis (2021)
592 Systematic and collaborative approach to problem solving using X-ray photoelectron
593 spectroscopy. Applied Surface Science Advances, 5, 100112.
594 Filiberto, J., and Treiman, A.H. (2009) The effect of chlorine on the liquidus of basalt: First
595 results and implications for basalt genesis on Mars and Earth. Chemical Geology, 263, 60-68.
596 Finger, L.W., and King, H.E. (1978) A revised method of operation of the single-crystal
597 diamond cell and refinement of the structure of NaCl at 32 kbar. American Mineralogist, 63,
598 337-342
599 Gin, S., Abdelouas, A., Criscenti, L.J., Ebert, W.L., Ferrand, K., Geisler, T., Harrison, M.T.,
600 Inagaki, Y., Mitsui, S., Mueller, K.T., et al. (2013) An international initiative on long-term
601 behavior of high-level nuclear waste glass, Materials Today, 16, 243-248.
602 Gin, S., Jollivet, P., Tribet, M., Peuget, S., and Schuller, S. (2017). Radionuclides
603 containment in nuclear glasses: An overview. Radiochimica Acta, 105, 927–959.
604 Goel, A., McCloy, J.S., Pokorny, R., and Kruger, A.A. (2019). Challenges with vitrification
605 of Hanford High-Level Waste (HLW) to borosilicate glass – An overview. Journal of Non-
606 Crystalline Solids: X, 4, 100033.
607 Guerette M., and Huang, L. (2015) In-situ Raman and Brillouin light scattering study of the
608 international simple glass in response to temperature and pressure. Journal of Non-Crystalline
609 Solids 411, 101-105.
610 Herd, C.D.K., Borg, L.E., Jones,J.H., and Papike, J.J. (2002) Oxygen fugacity and
611 geochemical variations in the martian basalts: Implications for martian basalt petrogenesis and
612 the oxidation state of the upper mantle of Mars. Geochimica and Cosmochimica Acta, 66,
613 2025-2036.

614 Hmra, P. (2010) Retention of Halogens in Waste Glass. U.S. department of energy, Pacific
615 Northwest National Laboratory, PNNL-19361.
616 Ilyukhina, N.S., Panomaryova, I.Y., Lashchenova, T.N., and Stefanovsky, S.V. (2010).
617 Solubility of sulfate and chloride ions in borosilicate melts at vitrification of intermediate-
618 level radioactive wastes, in: WM2010 Conference, Phoenix.
619 Inagaki, Y., Kikunaga, T., Idemitsu, K., and Arima, T. (2013) Initial dissolution rate of the
620 International Simple Glass as a function of pH and temperature measured using microchannel
621 flow-through test method, Journal of Applied Glass Science, 4, 317-327.
622 Inagaki, Y. (2014) Micro-channel as a new tool to investigate glass dissolution kinetics.
623 Proceeding in Material Science, 7, 172-178.
624 Johnston, D. (1980) Volcanic contribution of chlorine to the stratosphere: More significant to
625 ozone that previously estimated? Science, 209, 491-492.
626 Jolivet, V., Jossé, L., Rivoal, M., Paris, M., Morizet, Y., Carole, L., and Suzuki-Muresan, T.
627 (2019) Quantification of boron in aluminoborosilicate glasses using Raman and ^{11}B NMR.
628 Journal of Non-Crystalline Solids, 511, 50-61.
629 Jolivet, V., Morizet, Y., Paris, M., and Suzuki-Muresan, T. (2020) High pressure experimental
630 study on iodine solution mechanisms in nuclear waste glasses, Journal of Nuclear. Materials,
631 533, 152112 .
632 Jolivet, V., Morizet, Y., Hamon, J., Paris, M., and Suzuki-Muresan, T. (2021) the influence of
633 iodide on glass transition temperature of high-pressure waste glasses. Journal of the American
634 Ceramic Society, 104, 1360-1369.
635 Jugo, P.J., Wilke, M., and Botcharnikov, R.E. (2010) Sulfur K-edge XANES analysis of
636 natural and synthetic basaltic glasses: Implications for S speciation and S content as function
637 of oxygen fugacity. Geochimica and Cosmochimica Acta, 74, 5926-5938.

638 Karan, N.K., and Arunan, E. (2004) Chlorine bond distances in ClF and Cl_2 complexes.
639 Journal of Molecular Structure, 688, 203-205.
640 Kelsey, K.E., Allwardt, J.R., and Stebbins, J.F. (2008) Ca-Mg mixing in aluminosillicate
641 glasses: an investigation using ^{17}O MAS and 3QMAS and ^{27}Al MAS NMR. Journal of Non-
642 Crystalline Solids, 354, 4644–4653.
643 Klimm, K., Kohn, S.C., O'Dell, L.A., Botcharnikov, R.E., and Smith, M.E. (2012) The
644 dissolution mechanism of sulphur in hydrous silicate melts. I: assessment of analytical
645 techniques in determining the sulphur speciation in iron-free to iron-poor glasses. Chemical
646 Geology, 322-323, 237–249.
647 Landrot G. (2018) FASTOSH: A software to process XAFS data for geochemical and
648 environmental applications. Goldschmidt Abstract, 1402.
649 Langowski, M.H., Darab, J.G., and Smith, P.A. (1996) Volatility literature of chlorine, iodine,
650 cesium, strontium, technetium, and rhenium; technetium and rhenium volatility testing. U.S.
651 department of energy, Pacific Northwest National Laboratory, PNNL-11052.
652 McKeown, D.A., Gan, H., Pegg, I.L., Stolte, W.C., and Demchenko, I.N. (2011). X-ray
653 absorption studies of chlorine valence and local environments in borosilicate waste glasses.
654 Journal of Nuclear Materials, 408, 236–245.
655 Mendoza C., Peuget S., Bouty O., Caraballo R., and Jégou C. (2012) Simplified nuclear
656 glasses structure behaviour under various irradiation conditions: a Raman spectroscopy study.
657 Proceeding in Chemistry, 7, 581-586.
658 Méplan, O., and Nuttin A. (2006) La gestion des déchets nucléaires. Images de la Physique, 9-
659 17.
660 Metcalfe, B.L., and Donald, I.W. (2004) Candidate wasteforms for the immobilization of
661 chloride-containing radioactive waste. Journal of Non-Crystalline Solids, 348, 225–229.

662 Métrich, N., and Rutherford, M.J. (1992) Experimental study of chlorine behavior in hydrous
663 silicic melts. Geochimica and Cosmochimica Acta, 56, 607–616.
664 Mohd Fadzil, S., Hrma P., Schweiger M.J., and Riley B.J. (2015) Liquidus temperature and
665 chemical durability of selected glasses to immobilize rare earth oxides waste. Journal of
666 Nuclear Materials, 465, 657-663.
667 Morizet, Y., Paris, M., Gaillard, F., and Scaillet, B. (2010) C-O-H fluid solubility in
668 haplobasalt under reducing conditions: an experimental study. Chemical Geology, 279, 1–16.
669 Morizet, Y., Paris, M., Sifré, D., Di Carlo, I., Ory, S., and Gaillard, F. (2017) Towards the
670 reconciliation of viscosity change and CO_2-induced polymerization in silicate melts. Chemical
671 Geology, 458, 38-47.
672 Morizet, Y., Hamon, J., La, C., Jolivet, V., Suzuki-Muresan, T., and Paris, M. (2021a)
673 Immobilization of ^{129}I in nuclear waste glass matrixes synthesized under high-pressure
674 conditions: an experimental study. Journal of Materials Chemistry A, 9, 23902.
675 Morizet, Y., Jolivet, V., Trcera, N., Suzuki-Muresan, T., and Hamon, J. (2021b) Iodine local
676 environment in high pressure borosilicate glasses: An X-ray photoelectron spectroscopy and
677 X-ray absorption spectroscopy investigation. Journal of Nuclear Materials, 553, 153050.
678 Moulder, J.F., Stickle, W.F., Sobol, P.E., and Bomben, K.D. (1992) Handbook of W-ray
679 Photo- electron Spectroscopy: a reference book of standard spectra for identification and
680 interpretation of XPS spectra, J. Chastain Ed., Perkin-Elmer Corporation Physical Electronics
681 Division, Eden Prairie, Minnesota.
682 Newbury, D.E., and Ritchie, N.W.M. (2013) Is scanning electron microscopy/energy
683 dispersive X-ray spectrometry (SEM/EDS) quantitative? Scanning, 35, 141-168.
684 Newville, M., Ravel, B., Haskel, D., Rehr, J.J., Stern, E.A., and Yacoby, Y. (1995) Analysis
685 of multiple-scattering XAFS data using theoretical standards. Physica B, 208/209, 154–156.

686 Ojovan, M.I., and Lee, W.E. (2011) Glassy wasteforms for nuclear waste immobilization.
687 Metallurgical and Materials Transactions A: Physical Metallurgy and Materials Science, 42,
688 837–851.
689 Paul, D.K., Buckley, F., and Nixon, P.H. (1976) Fluorine and chlorine geochemistry of
690 kimberlites. Chemical Geology, 17, 125-133.
691 Pawley, A.R., Holloway, J.R., and McMillan, P.F. (1992) The effect of oxygen fugacity on
692 the solubility of carbon–oxygen fluids in basaltic melt. Earth Planetary Science Letter, 110,
693 213–225.
694 Ravel, B., and Newville, M. (2005) ATHENA, ARTHEMIS, HEPHAESTUS: data analysis
695 for Xray absorption spectroscopy using IFEFFIT. Journal of Synchrotron Radiation, 12, 537–
696 541.
697 Riley, B.J., Vienna, J.D., Strachan, D.M., McCloy, J.S., and Jerden Jr., J.L. (2016) Materials
698 and processes for the effective capture and immobilization of radioiodine: a review. Journal of
699 Nuclear Materials, 470, 307–326.
700 Roux, C., Le Gal La Salle, C., Simonucci, C., Van Meir, N., Fifield, L. K., Bourlès, D. L., and
701 Lancelot, J. (2014) High ^{36}Cl/Cl ratios in Chernobyl groundwater. Journal of Environmental
702 Radioactivity, 138, 19–32.
703 Schofield, J.M., Bingham, P.A., and Hand, R.J. (2009) The immobilisation of a chloride
704 containing actinide waste surrogate in calcium aluminosilicate glasses, in: A. Cozzi, T. Ohji
705 (Eds.), Environmental Issues and Waste Management Technologies in the Materials and
706 Nuclear Industries XII, John Wiley & Sons, Inc, pp. 69-80.
707 Shannon, R.D. (1976) Revised effective ionic radii and systematic studies of interatomic
708 distances in halides and chalcogenides. Acta Crystallographia, A32, 751-767.

709 Signorelli, S., and Carroll, M.R. (2002) Experimental study of Cl solubility in hydrous
710 alkaline melts: constraints on the theoretical maximum amount of Cl in trachytic and
711 phonolitic melts. Contribution to Mineralogy and Petrology, 143, 209–218.
712 Siwadamrongpong, S., Koide, M., and Matusita, K. (2004) Prediction of chloride solubility in
713 CaO-Al_2O_3-SiO_2 glass systems. Journal of Non-Crystalline Solids, 347, 114–120.
714 Symonds, R.B., Rose, W.I., and Reed, M.H. (1988) Contribution of Cl- and F-bearing gases
715 to the atmosphere by volcanoes, Nature, 334, 415-418.
716 Tan, S. (2015). The incorporation and solubility of sulphate, chloride and molybdate anions in
717 borosilicate and aluminosilicate glasses. Immobilisation Science Laboratory, pp. 254.
718 Tan, S., and Hand, R.J. (2018) Incorporation and phase separation of Cl in alkaline earth
719 aluminosilicate glasses. Journal of Nuclear Materials, 507, 135–144.
720 Thomas, R.W., and Wood, B.J. (2021) The chemical behaviour of chlorine in silicate melts.
721 Geochimica et Cosmochimica Acta, 294, 28–42.
722 Tomilin, S.V., Lukinykh, A.N., Lizin, A.A., Bychkov, A.V., Yakovlev, V.V., and Konovalov,
723 V.I. (2007) Investigation of the incorporation of spent alkali chloride melt in ceramic. Atomic
724 Energy, 102, 217–222.
725 Tougaard, S. (1997) Universality classes of inelastic electron scattering cross-sections.
726 Surface Interface Analysis, 25, 137–154.
727 Vaitkus, A., Merkys, A., and Grazulis, S. (2021) Validation of the Crystallographic Open
728 Database using the Crystallographic Information Framework. Journal of Applied
729 Crystallography, 54, 661-672.
730 Vance, E.R., Davis, J., Olufson, K., Chironi, I., Karatchevtseva, I., and Farnan, I. (2012)
731 Candidate waste forms for immobilisation of waste chloride salt from pyroprocessing of spent
732 nuclear fuel. Journal of Nuclear Materials, 420, 396–404.

733 Vantelon, D., Trcera, N., Roy, D., Moreno, T., Mailly, D., Guillet, S., Metchalkov, E.,
734 Delmotte, F., Lassalle, B., Lagarde, P., and Flank, A.M. (2016) The LUCIA beamline at
735 SOLEIL. Journal of Synchrotron Radiation, 23, 635–640 .
736 Webster, J.D., Kinzler, R.J., and Mathez, A. (1999) Chloride and water solubility in basalt
737 and andesite melts and implications for magmatic degassing. Geochimica and Cosmochimica
738 Acta, 63, 729-738.
739 Webster, J. D., Goldoff, B., Sintoni, M. F., Shimizu, N., and De Vivo, B. (2014) C-O-H-Cl-S-
740 F volatile solubilities, partitioning, and mixing in phonolitic trachytic melts and aqueous-
741 carbonic vapor ± saline liquid at 200 MPa. Journal of Petrology, 55, 2217–2248.
742 Webster, J.D., Vetere, F., Botcharnikov, R.E., Goldoff, B., McBirney, A., and Doherty, A.L.
743 (2015) Experimental and modeled chlorine solubilities in aluminosilicate melts at 1 to 7000
744 bars and 700 to 1250 °C: Applications to magmas of Augustine Volcano, Alaska. American
745 Mineralogist, 100, 522–535.
746 Webster, J.D., Baker, D.R., and Aiuppa, A. (2018) Halogens in mafic and intermediate-silica
747 content magmas. In: Harlov D., Aranovich L.Y. (Eds.), The Role of Halogens in Terrestrial
748 and Extraterrestrial Geochemical Processes: Surface, Crust and Mantle. Springer Lectures in
749 Geology Series, pp. 307–430.
750 Webster, J.D., Iveson, A.A., Rowe, M.C., and Webster, P.M. (2020) Chlorine and felsic
751 magma evolution: Modelling the behavior of an under-appreciated volatile component.
752 Geochimica and Cosmochimica Acta, 271, 248-288.
753 Wells, A.F. (1938) The Crystal Structure of Palladous Chloride $PdCl_2$. Zeitschrift fuer
754 Kristallographie, Kristallgeometrie, Kristallphysik, Kristallchemie, 100, 189-194.

Wetzel, D.T., Rutherford, M.J., Jacobsen, S.D., Hauri, E.H., and Saal, A.E. (2013) Degassing of reduced carbon from planetary basalts. Proceedings of the National Academy of Science, 110, 8010-8013.

Wickham, A., Steinmetz, H.J., O'Sullivan, P., and Ojovan, M.I. (2017). Updating irradiated graphite disposal: Project 'GRAPA' and the international decommissioning network. Journal of Environmental Radioactivity, 171, 34–40.

Wilke, M., Klimm, K., and Kohn, S.C. (2011) Spectroscopic studies on sulfur speciation in synthetic and natural glasses. In H. Behrens and J.D. Webster, Eds., Sulfur in Magmas and Melts: Its Importance for Natural and Technical Processes, 73, p. 41–78. Reviews in Mineralogy and Geochemistry, Mineralogical Society of America, Chantilly, Virginia.

Zhao, W., Li, K., Lin, P., Xu, K., and Tan, S. (2019) Dissolution of Cl in alkaline earth (Ca, Sr, Ba) aluminosilicate glasses. Journal of Non-Crystalline Solids, 516, 56–62.

Zachariasen, W.H. (1929) The Crystal Structure of Sodium Chlorate. Zeitschrift fuer Kristallographie, Kristallgeometrie, Kristallphysik, Kristallchemie, 71, 517-529.

Zimova, M., and Webb, S.L. (2007) The combined effects of chlorine and fluorine on the viscosity of aluminosilicate melts. Geochimica et Cosmochimica Acta, 71, 1553–1562.

Figure caption

Figure 1: Chlorine content as a function of non-network former cations content expressed as the [CaO + Na_2O] showing the gradual increase in Cl solubility with increasing network modifying cation concentration.

Figure 2: Change in Cl solubility as a function of XCaO = [CaO] / [CaO + Na_2O]. It can be clearly observed that Cl solubility is enhanced in the case of Ca-rich glasses in comparison to Na-rich suggesting that the nature of the cation itself plays a major role on Cl solubility.

779 Figure 3: Cl K-edge XANES spectra acquired for glasses (A) and crystalline compounds (B).
780 The used source of chlorine is indicated for Cl-bearing glasses.
781 Figure 4: XPS spectra in the Cl 2p binding energy region and obtained for several glasses
782 with different Cl content up to 11.1 mol.%. Chlorine is dissolved only as chloride species as
783 witnessed by the doublet peak located at ~200 eV. The peak fitting parameters are indicated
784 next to each simulation. There is no evidence of chlorate species.
785 Figure 5: Radial Distribution Function (R+ΔR in Å) obtained from EXAFS spectra for glasses
786 with different Cl content. The insert corresponds to the imaginary part of the RDF amplitude
787 spectrum. The fitted region is indicated and does not consider the lower R+ΔR signal that is
788 considered as an unwanted EXAFS signal and basically filtered (see Suppl. Mat. 2).
789 Figure 6: Chlorine solubility (in mol.%) as a function of the Network Modifying Field
790 Strength (see text for the detailed calculation). Along to this work, several other datasets are
791 also reported: Filiberto and Treiman (2009), Dalou et al. (2015), Webster et al. (2015). The
792 trends in the data of Dalou et al. (2015) is ascribed to the difference in the Al_2O_3 content; the
793 lower chlorine solubility for Filiberto and Treiman (2009) can be explained by the reducing
794 conditions applied during their experiments.

This is the peer-reviewed, final accepted version for American Mineralogist, published by the Mineralogical Society of America.
The published version is subject to change. Cite as Authors (Year) Title. American Mineralogist, in press.
DOI: https://doi.org/10.2138/am-2022-8599. http://www.minsocam.org/

Table 1: Experimental conditions, major element concentrations and chlorine solubility in synthesized glasses.

Sample	T (°C)	P (GPa)	Duration (h)	$Cl^{init.d}$	SiO_2	Al_2O_3	B_2O_3	CaO	Na_2O	ZrO_2	Total	$Cl^{sol.}$	K*[a]	R*[a]	XCaO[b]	NMFS[c]
					Mol.%[e]											
ISG21-1 $PdCl_2$	1400	0.5	5	11.4	64.6	4.0	17.5	4.5	5.2	1.9	97.7	2.3	3.9	0.6	0.46	1.70
ISG21-2 $PdCl_2$	1400	0.5	5	27.2	60.0	3.8	16.9	5.6	8.7	1.8	96.7	3.3	3.8	0.3	0.39	1.74
ISG22-1 $PdCl_2$	1400	1	5	17.1	64.6	4.0	17.8	4.0	5.1	2.0	97.5	2.5	3.9	0.5	0.44	1.70
ISG22-2 $PdCl_2$	1400	1	5	29.1	61.5	3.8	16.9	5.0	7.5	2.0	96.8	3.2	3.9	0.3	0.4	1.72
ISG23-1 $PdCl_2$	1400	1.5	5	15.6	63.1	4.0	18.6	4.4	5.2	2.0	97.3	2.7	3.6	0.6	0.46	1.72
ISG23-2 $PdCl_2$	1400	1.5	5	22.3	61.2	3.8	16.4	5.2	7.8	2.0	96.4	3.6	4.0	1.0	0.4	1.72
ISG22-1 NaCl	1400	1	5	4.4	57.1	3.6	15.2	5.5	13.7	1.6	96.6	3.4	4.0	1.0	0.29	1.78
ISG22-2 NaCl	1400	1	5	6.5	57.0	3.6	15.2	5.4	13.7	1.6	96.5	3.5	4.0	1.0	0.28	1.78
ISG22-3 NaCl	1400	1	5	11.3	56.9	3.6	15.3	5.4	13.7	1.5	96.4	3.6	4.0	3.2	0.28	1.78
LJ8 221 NaCl	1400	1	5	3.5	62.3	6.0	5.4	7.9	15.6		97.1	2.9	12.7	2.7	0.34	1.70
LJ8 222 NaCl	1400	1	5	6.9	61.1	5.8	6.0	7.8	15.5		96.2	3.8	11.2	2.8	0.33	1.71
LJ8 021 NaCl	1200	1	1	6.5	60.5	5.4	6.7	8.0	15.2		95.8	4.2	9.9	2.8	0.34	1.71
BASN3-211 NaCl	1400	0.5	4	3.8	62.4	9.8	4.4		22.3		98.9	1.1	16.2	3.1	0	1.81
BASN3-212 NaCl	1400	0.5	4	11.5	62.3	9.8	4.4		22.3		98.9	1.1	16.2	3.6	0	1.81
BASN3 221 NaCl	1400	1	5	3.8	61.6	9.7	4.4		23.0		98.7	1.3	16.1	3.3	0	1.82
BASN3 223 NaCl	1400	1	5	11.5	61.3	9.6	4.4		23.3		98.6	1.4	16.0	1.6	0	1.82
BASN3-231 NaCl	1400	1.5	4	3.8	63.7	9.7	3.1		20.8		97.4	2.6	23.4	0.9	0	1.78
BASN3-232 NaCl	1400	1.5	4	11.5	63.2	9.1	3.7		21.2		97.3	2.7	19.7	0.4	0	1.79
BASN3-021 NaCl	1200	1	1	6.3	61.6	8.2	7.2		19.6		96.6	3.4	9.6	0.8	0	1.80
NH21-1 $PdCl_2$	1400	0.5	5	13.3	46.0	9.8	15.9	7.9	16.9		96.5	3.5	3.5	1.8	0.32	1.92
NH21-2 $PdCl_2$	1400	0.5	5	24.6	55.5	9.0	15.6	6.4	9.6		96.2	3.8	4.1	1.7	0.4	1.81
NH22-1 $PdCl_2$	1400	1	5	13.7	49.4	10.5	13.5	7.8	13.3		94.5	5.5	4.4	2.1	0.37	1.86
NH22-2 $PdCl_2$	1400	1	5	26.3	44.7	9.5	13.5	7.7	18.7		94.0	6.0	4.0	2.0	0.29	1.92
NH22-2 NaCl	1400	1	5	7.3	40.9	9.0	13.4	7.6	25.5		96.4	3.6	3.7	0.5	0.23	1.99
NH22-3 NaCl	1400	1	5	12.0	39.0	8.8	13.7	7.0	25.1		93.6	6.4	3.5	1.7	0.22	2.01
BFS3-222 NaCl	1400	1	5	11.7	41.1	5.4	12.4	25.6	5.3		89.8	10.2	3.8	0.7	0.83	1.69
BFS4-221 NaCl	1400	1	5	7.7	46.1	6.0	11.8	18.9	10.7		93.5	6.5	4.4	0.5	0.64	1.75
pCABS1-Cl $PdCl_2$	1350	1	4	15.2	50.6	5.5	21.8	16.1			94.0	6.1	2.6	0.6	1	1.74
pCABS2-Cl $PdCl_2$	1350	1	4	10.0	44.5	5.1	13.4	27.4			90.4	9.6	3.7	0.5	1	1.63
C35-Cl $PdCl_2$	1350	1	4	14.5	28.2	4.8	29.7	26.2			88.9	11.1	1.1	0.6	1	1.87
LJ4b-223 NaCl	1400	1	5	11.4	48.1		31.3		16.6		96.0	4.0	1.5	1.0	0	1.98

[a] The K* and R* parameters are derived from the parameters defined by Dell et al. (1983) for Na-bearing borosilicate glasses and have been modified in order to introduce the presence of Al_2O_3 and the presence of CaO. See text for the details on the calculations.

[b] The XCaO is defined as the ratio between CaO and the total network modifying cation concentration such as [CaO] / [CaO + Na_2O].

[c] The NMFS corresponds to the Network Modifying Field Strength that is calculated from Eq. 1. It stands for the field strength (z_i/r_i) of the network modifying cations (Ca^{2+} and Na^{+}) normalized to the field strength of the total oxygen carried by the network modifying cations.

[d] The $Cl^{init.}$ indicates the initial loaded chlorine content in the capsule either as NaCl or $PdCl_2$.

[e] The major element concentrations including the chlorine solubility have been determined using SEM-EDS and the B_2O_3 content is calculated from the total and corrected according to the ISG standard (see Jolivet et al. 2020). The typical error bar on each oxide and chlorine is ±0.2 mol.%.

This is the peer-reviewed, final accepted version for American Mineralogist, published by the Mineralogical Society of America.
The published version is subject to change. Cite as Authors (Year) Title. American Mineralogist, in press.
DOI: https://doi.org/10.2138/am-2022-8599. http://www.minsocam.org/

Table 2: Cl K-edge EXAFS spectra simulation results for chlorine local atomic environment in glasses.

Sample	$Cl^{sol.}$	R space (Å)[a]	CN_{Cl-Pd}	r_{Cl-Pd}	s_{Cl-Pd}	CN_{Cl-Na}	r_{Cl-Na}	s_{Cl-Na}	CN_{Cl-Ca}	r_{Cl-Ca}	s_{Cl-Ca}
LJ4b-223	4.0	1.5-2.8				2.46(14)[b]	2.70(0)	0.012(1)			
BASN3-212	1.1	1.5-2.8				3.63(26)	2.67(1)	0.023(1)			
BFS3-222[d]	10.2	1.75-2.9				0.44(14)	2.52(2)	0.007(4)	0.68(17)	2.77(2)	0.015(4)
ISG23-2	3.6	1.1-3.0	1.97(6)	2.30(0)	0.012(0)	5.91(32)	2.68(1)	0.036(1)	0.63(5)	2.74(1)	0.008(1)
NH22-2 $PdCl_2$	6.0	1.7-3.0	0.42(9)	2.15(2)	0.014(2)	8.86(88)	2.64(3)	0.076(6)	0.40(4)	2.80(1)	0.001(0)
pCABS2-Cl	9.6	1.75-2.8	0.72(20)	2.46(3)	0.023(4)				1.73(11)	2.72(1)	0.017(1)
C35-Cl[c]	11.1	1.75-2.8	0.51(15)	2.23(2)	0.016(4)				1.95(16)	2.70(1)	0.018(1)

[a] The R space corresponds to the Radial Distribution Function interval obtained from EXAFS that has been fitted.
[b] The error derived on each fitted parameter is reported in between the brackets and corresponds to a variation on the last digit value. The error has been from the Artemis fitting software.
[c] For this particular sample, we observe a strong signal not averaged out by the R background (see Suppl. Mat.) located at ~1.3 Å, which could correspond to a distance to first neighbor on the order of ~1.8 Å. Although, we did not try to simulate this peak we ascribe it to the possible presence of bubbles filled with gaseous Cl_2 with r_{Cl-Cl} = 1.8 Å.
[d] The reported data for this sample is uncertain considering the possibility for Na^+ and Ca^{2+} to be in the vicinity of the Cl^- species. Hence, the simulations using either Cl-Na path or Cl-Ca path or both Cl-Na and Cl-Ca paths lead to very similar results. In other words, the distinction between the Ca or Na local environments surrounding the Cl^- is not possible.

This is the peer-reviewed, final accepted version for American Mineralogist, published by the Mineralogical Society of America.
The published version is subject to change. Cite as Authors (Year) Title. American Mineralogist, in press.
DOI: https://doi.org/10.2138/am-2022-8599. http://www.minsocam.org/

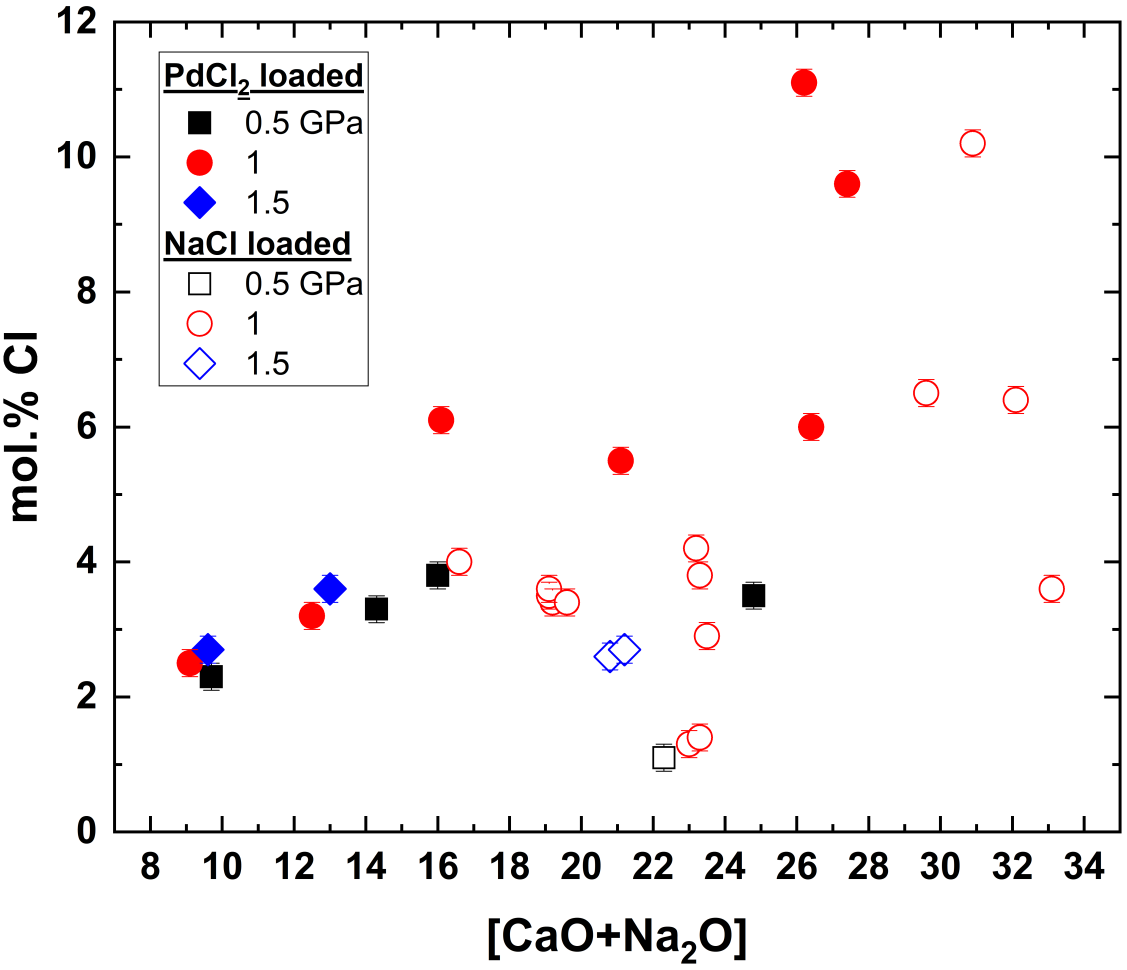

Figure 1

This is the peer-reviewed, final accepted version for American Mineralogist, published by the Mineralogical Society of America.
The published version is subject to change. Cite as Authors (Year) Title. American Mineralogist, in press.
DOI: https://doi.org/10.2138/am-2022-8599. http://www.minsocam.org/

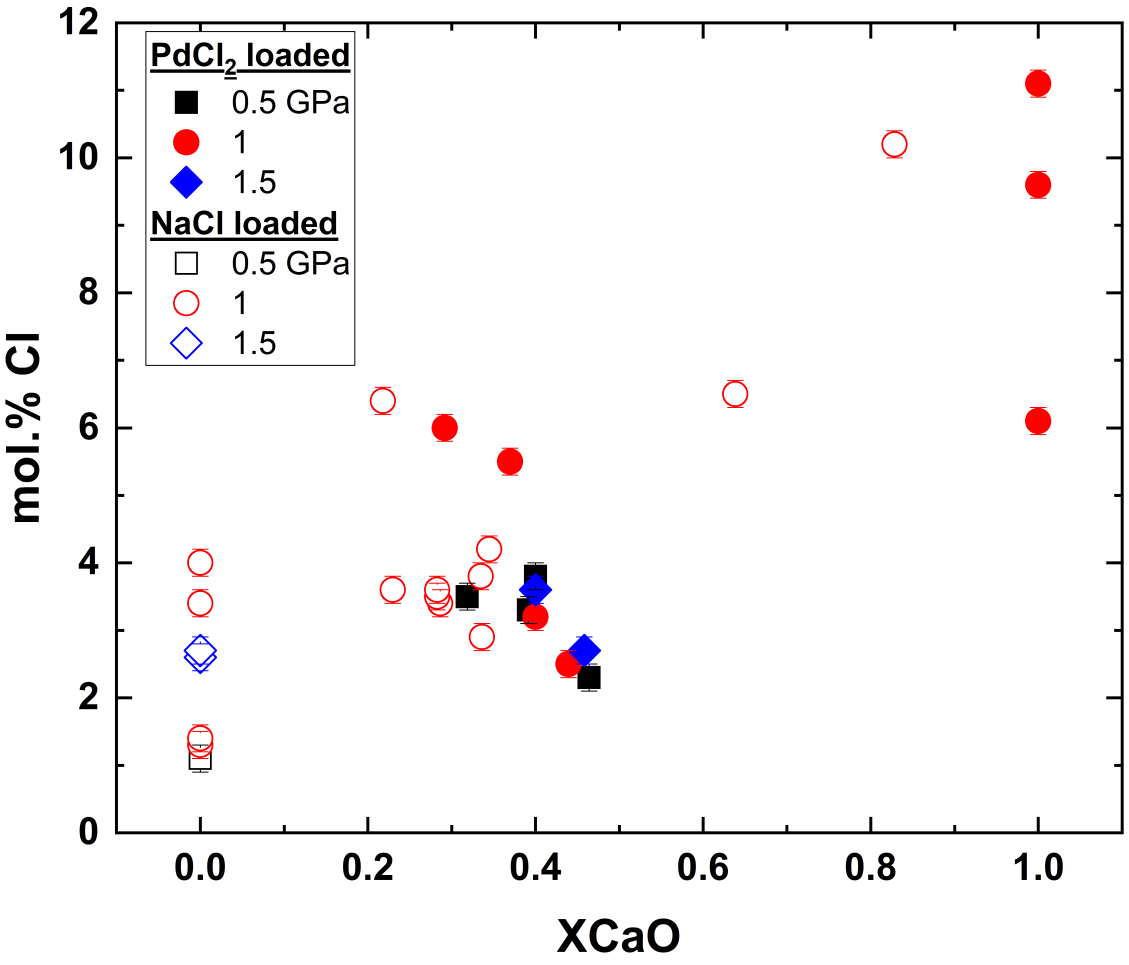

Figure 2

This is the peer-reviewed, final accepted version for American Mineralogist, published by the Mineralogical Society of America.
The published version is subject to change. Cite as Authors (Year) Title. American Mineralogist, in press.
DOI: https://doi.org/10.2138/am-2022-8599. http://www.minsocam.org/

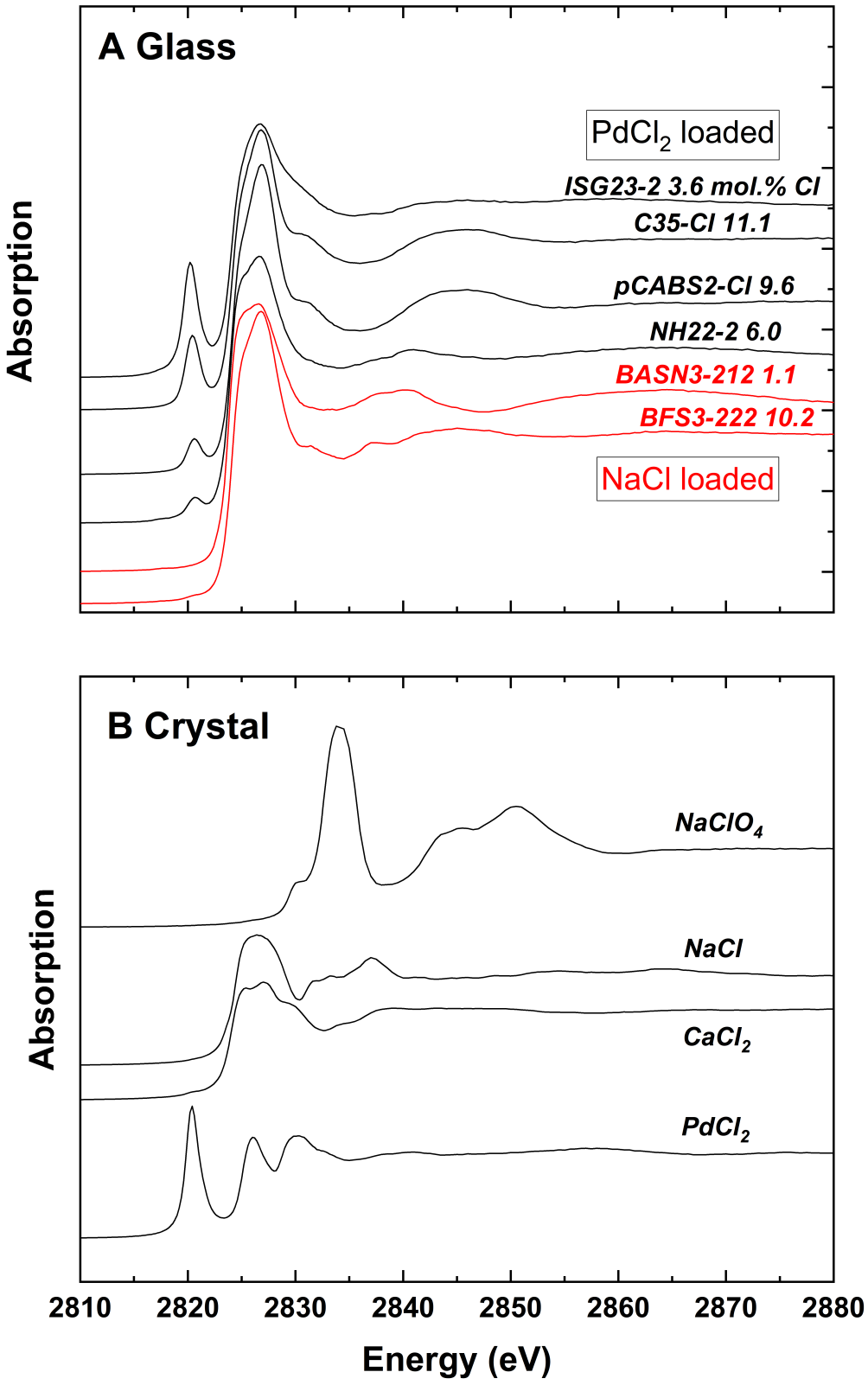

Figure 3

This is the peer-reviewed, final accepted version for American Mineralogist, published by the Mineralogical Society of America.
The published version is subject to change. Cite as Authors (Year) Title. American Mineralogist, in press.
DOI: https://doi.org/10.2138/am-2022-8599. http://www.minsocam.org/

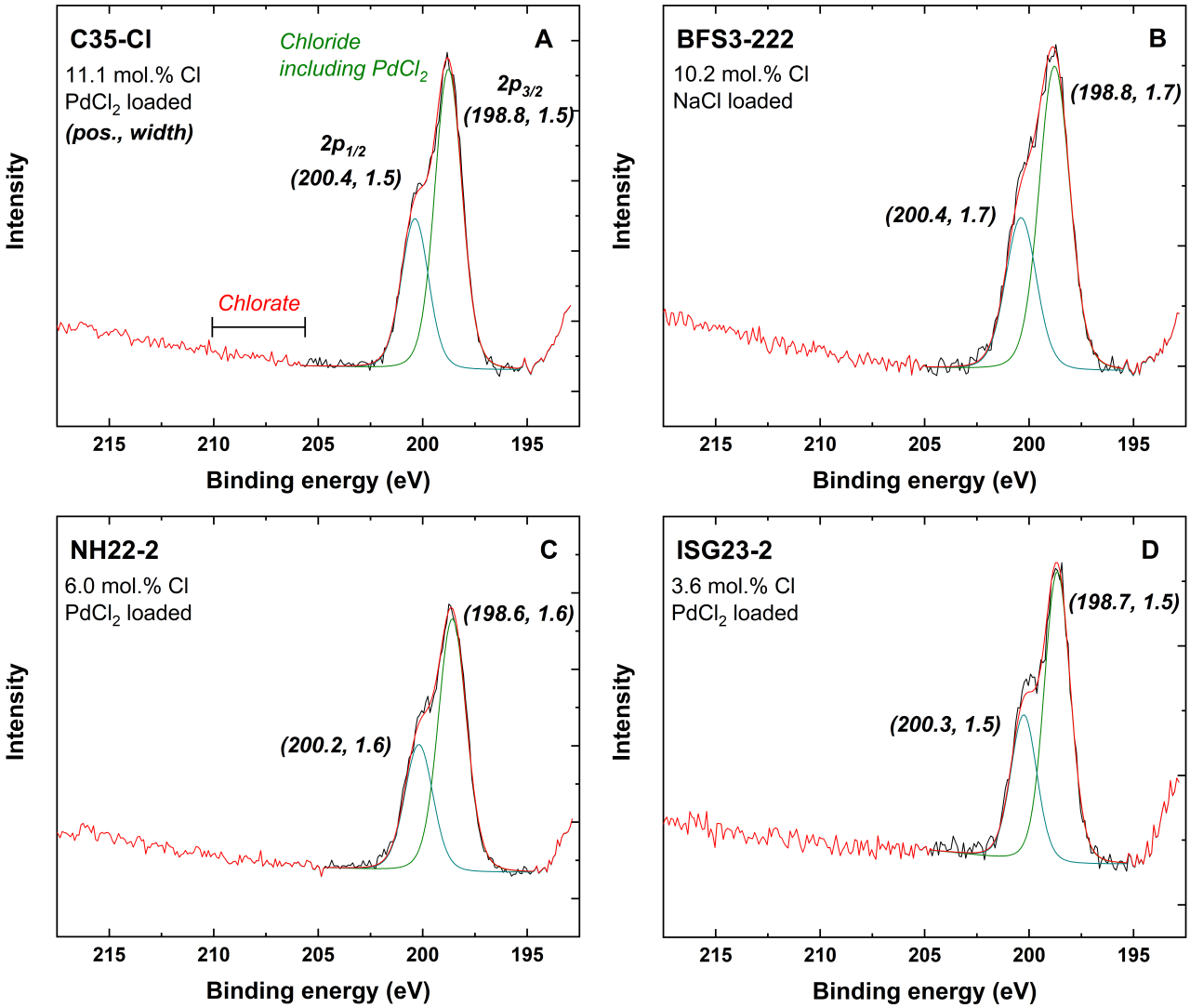

Figure 4

This is the peer-reviewed, final accepted version for American Mineralogist, published by the Mineralogical Society of America.
The published version is subject to change. Cite as Authors (Year) Title. American Mineralogist, in press.
DOI: https://doi.org/10.2138/am-2022-8599. http://www.minsocam.org/

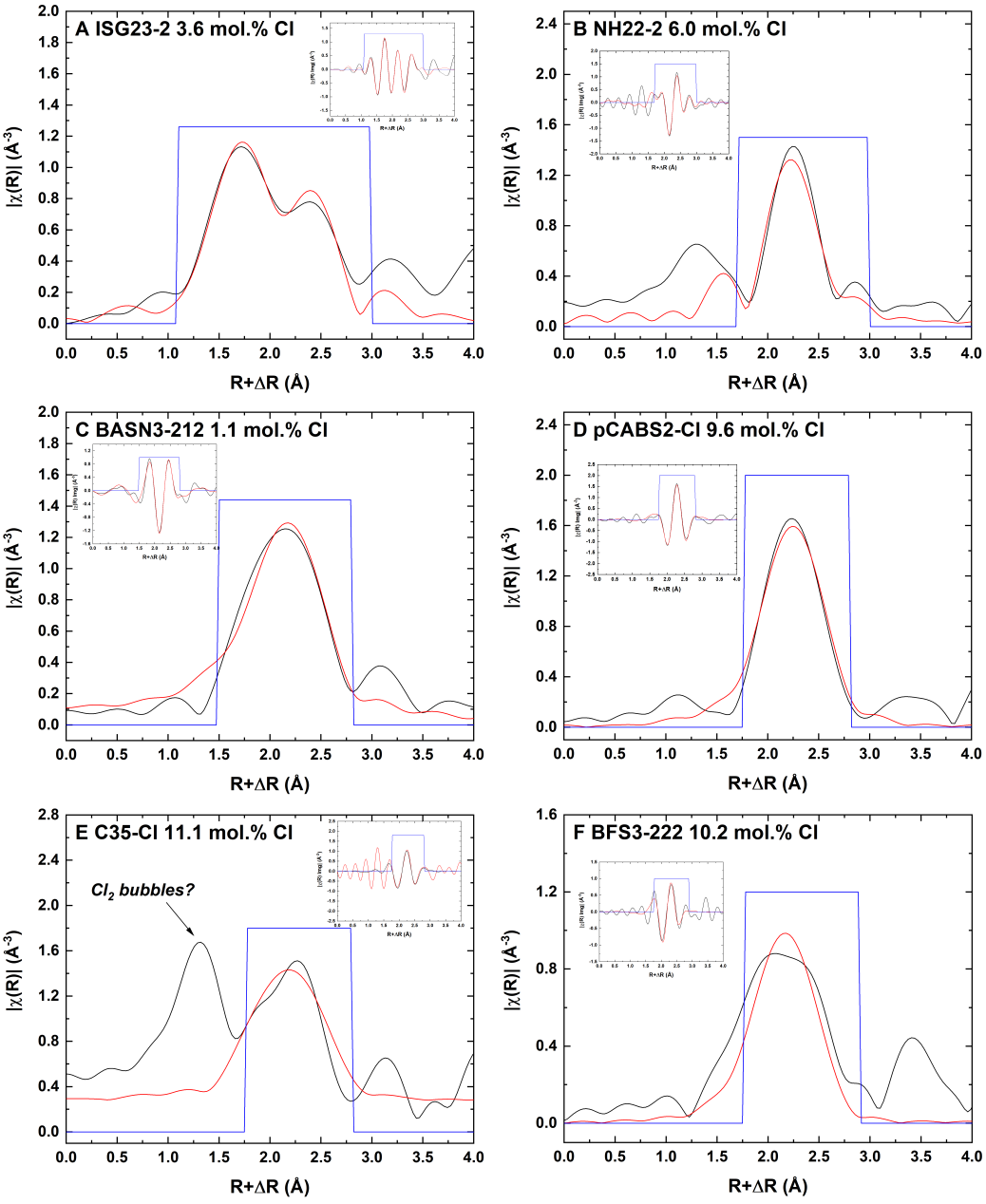

Figure 5

This is the peer-reviewed, final accepted version for American Mineralogist, published by the Mineralogical Society of America.
The published version is subject to change. Cite as Authors (Year) Title. American Mineralogist, in press.
DOI: https://doi.org/10.2138/am-2022-8599. http://www.minsocam.org/

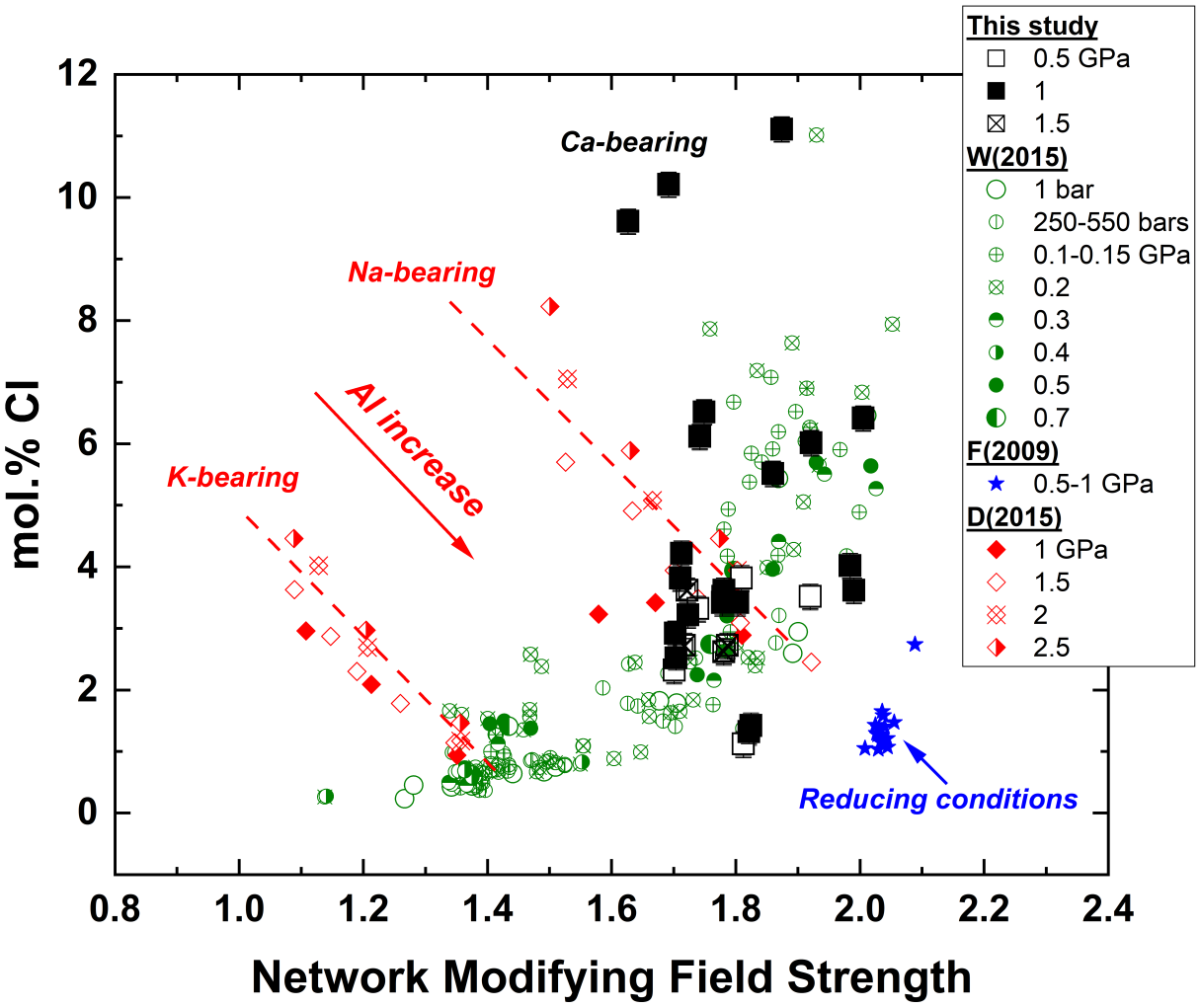

Figure 6